0.3 m. In order to obtain accurate data, water temperature was set a little bit higher than environmental temperature. That study took the vapor pressure ratio VP as evaluation index of diffusion effect, specific is defined as follow:

$$VP = (e-e_0) / (e_s-e_0) \qquad (1)$$

Where e is the vapor pressure at measuring point (Pa), e_0 is the vapor pressure at the base point (Pa), e_s is the saturated vapor pressure related to water temperature (Pa).
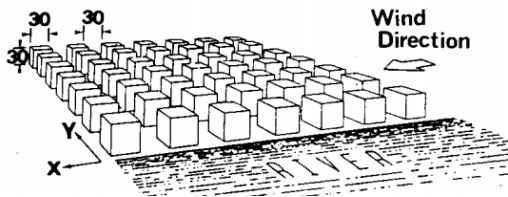

Figure 1 Workstation in windtunnel

Figure 2 Blocks distribution in models

CFD modelling scheme

At the inflow boundary, a velocity profile for the atmospheric boundary layer was applied. The velocity profile was constructed using a power law with the parameters provided by windtunnel experiment and the vertical profile for turbulent kinetic energy was constructed based on measured data. Vortex method was used in LES model. Semi-empirical expression was used in SKE model, low-ke model and RSM to related turbulence energy k, the dissipate rate of turbulent kinetic energy ε and turbulence intensity in windtunnel test. The expressions related were as follows:

$$I(z) = 0.1(Z / Z_G)^{(-\alpha-0.05)} \qquad (2)$$

$$K(z) = (I(z) \cdot U(z))^2 \qquad (3)$$

$$\varepsilon = C_\mu^{3/4} \cdot K \cdot \frac{dU}{dz} \qquad (4)$$

Where Z_G is boundary layer thickness, C_μ =0.09.

In order to guarantee good calculation accuracy and convergence stability, in this paper, we used five models which were S - A one-equation turbulence model SKE, low Reynolds number k-ε, RSM model

and LES turbulence model with changing mesh of structured grid according to the calculation demand. For instance, the minimum grid height near wall was 1/10 h when using wall function while 1/80 h in low Reynolds model. All setup conditions stayed the same with experimental conditions mentioned above. The simulation domain and mesh were shown as Figure 3.
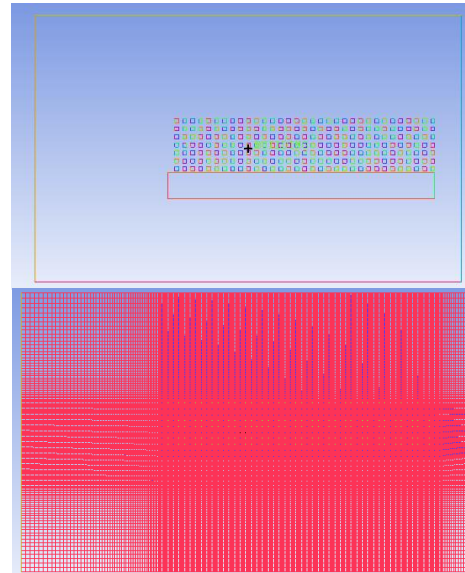

Figure 3 Simulation domain and mesh

Results and discussion

Figure 4 shows the distribution of water vapour mass fraction at the section of samplingsampling area calculated by each turbulence model. It is obvious that each figure shows different result of humidity distribution with each other, especially in the scale of diffusion above water body and in the building area. Compared with others, the result calculated by LES model seems to have higher level of humidity in building area and lower when above the water body.
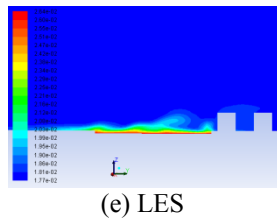

(a) S-A	(b) SKE

(c) Low-ke	(d) RSM

(e) LES
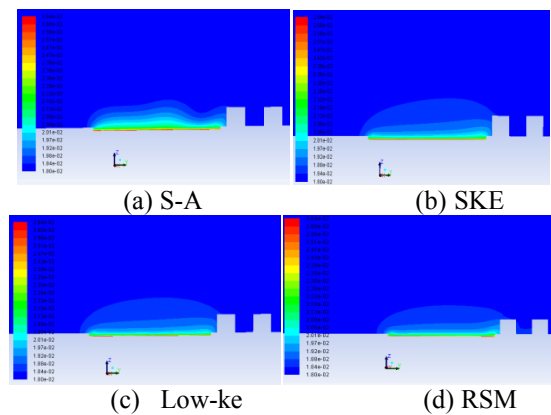
Figure 4. Distribution of water vapour mass fraction at the section of samplingsampling area

Figure 5 shows the results of differernt turbulence models comparing with windtunnel data. Horizontal ordinate value Y/W, in which Y represents distance from centre of water body, W represents the width of water body, shows the related location of measuring point. It can be seen that all models match the experimental data well. However, differernt model shows various trend with the distance increasing. The result calculated by LES shows the best agreement with the experimental data as expected. The next best is RSM model followed by SKE, of which prediction is higher above and around water body. By contrast, the result of low-ke model is much lower than experimental data in building area with distance ratio Y/W inceasing. The S-A model shows the worst performance of prediction on thermal enviroment as the result is higher around water body and lower in building area.
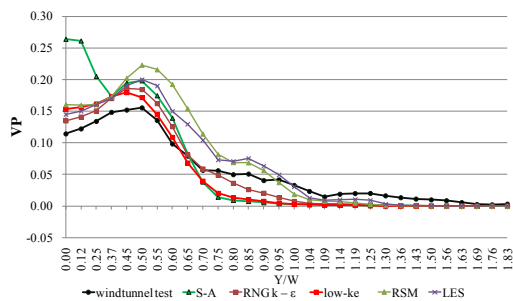

Figure 5 Results of different turbulence models

EVALUATION OF VARIOUS BUILDING DISTRIBUTIONS ALONG THE WATERFRONT

Physical models

According to the computational results of differernt models, SKE was found more suitable in solving full-scale case. Therefore, in this part SKE model was used to simulate four planning cases considering solar radiation and water body effection to predict wind and thermal-humidity environments in urban areas around unban water body. The layouts of those building arrays were shown in Figure 6, as we can see from that, a number of factors were taken into account such as water body size, distance from water

body, layouts of building arrays including differernt building shape, height, row and so on. In order to find regularities of thermal cliamte affected by distribution of buildings to large extent, vegetation was not considered in those models this time.

Climate characteristic in the northern region of china is hot in summer while very cold in winter, so the orientation of buildings mostly is toward south to acquire more sunshine. So in this paper, water body lined east-west direction infront of whole building area. Four plans will be discussed with differernt layouts. The main function of buildings in Case A was for commercial and residential use and the biggest building height was 84 m. The buildings of Case B were multi-storey plate-type and dot with the max. building height of 84 m; local enclosed type was adopted in Case C and Case D with differernt Building floor area ratio comparing with case A and Case B.

The water body lined on one side of the building district near the building with low height. The width of water body was 150 m and the first row of building was 120m away from river in all cases. The detailed information about each case listed in Table 1.

Table 1 Detail information about each case

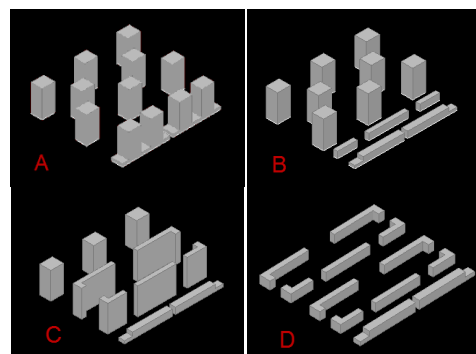| CASES	A	B	C	D
Building type	Dot	Dot and plate-type	Dot and enclosed-type	Dot and enclosed-type
Building floor area ratio	5.76	4.90	4.18	1.34
Building height in the front row (m)	104	20	20	20

Figure 6 Layouts of building arrays

CFD modelling scheme

According to climate data of Harbin in summer, the dominant wind direction was directly vertical to water body and average wind speed was 2.8m/s at the height of 10 metre. Steady-state simulation was carried out and the turbulence model using exponential distribution (Richards and Hoxey 1993). Solar radiation was simulated at 13:00 on June 30 with a sunny coefficient of 0.8. Temperatures and humidities of differernt underlyings were set separately.

In order to get the most accurate results of CFD simulation in a limited time, the SKE model was adopted to evaluate turbulence calculation in various cases comparing to other turbulence models in time and energy cost. At the lateral and upper surfaces of the computational domain, symmetry conditions were used, where normal velocity component and normal gradients of tangential velocity components set to zero. At the building surfaces and ground surface, the wall functions based on logarithmic laws were used. The thermal conductivity was 1.5 W/m•k and the heat transfer coefficient was set to 23 W/m^2•k. The external emissivity of the building array was 0.9 with wall roughness height of 2 m. Buildings and ground absorption of direct visible was 0.2 and 0.9 of the direct IR (Tanaka et al. 2000). At the outflow boundary, the zero gradient condition was used. The specific sets of models were illustrated in Table 2.

The computational domain size was about 1200 *1500*400m with about 2,500,000 structured grids (e.g. see Figure 7). Turbulence model used the standard k-ε model, pressure and speed coupled with SIMPLIC algorithm, The minimum grid width was 0.1 h. The QUICK scheme was applied for all convection terms.
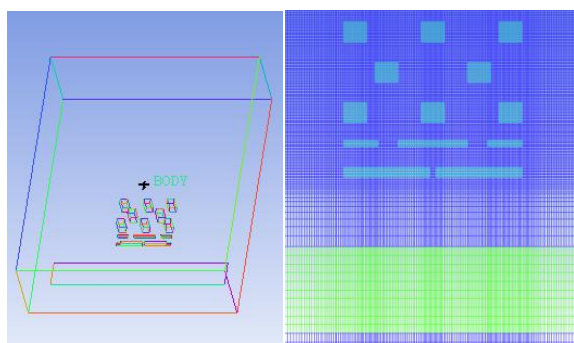

Figure 7 Simulation domain and mesh of Case B

Table 2 Main Boundary conditions

CONDITIONS	SETUP	EXPLANATION
Velocity	$u(z) = u(z_1)(\frac{z}{z_1})^\alpha$	α=0.25
Turbulence	$k = \frac{(u(z))^2}{C_\mu^{0.5}}$ $\varepsilon = \frac{C_\mu^{0.75} k^{\frac{3}{2}}}{\kappa z}$	C_μ=0.09；κ=0.4
Species transport	Mass fraction of water vapor	Water surface: 0.02269(kg/kg) Inlet airflow: 0.014785(kg/kg)
Temperature	constant	Inlet airflow: 31.2℃ Water body surface: 27.2℃
Solar radiation	Longitude:126.36° Latitude:45.44°	Direct solar radiation rate: 688W/m^2

Evaluation index

Referring to the type of evaluation intex of VP, two other indices which respectively take the temperature and himidity as main factor are proposed to evaluate the performance of differernt cases. The expressions were defined as follows:

$$t_V = (t\text{-}t_0) / (t_{in}\text{-}t_0) \qquad (5)$$

$$m_V = (m\text{-}m_0) / (m_{in}\text{-}m_0) \qquad (6)$$

where t is the temperature at measuring point (℃), t_0 is the temperature at the water surface (℃), t_{in} is the air temperature of inlet airflow (℃); m is the mass fraction of water vapor at measuring point, m_0 is the mass fraction of water vapor at water surface (℃), m_{in} is the mass fraction of water vapor of inlet airflow.

Results and discussion

As an example, Figure 8 shows temperature distribution in a longitudinal section of samplingsampling area in Case B. It can be seen that solar radiation flow is larger because of the higher sun altitude angle. The roofs and grounds which

expose to direct sunlight are impacted greater by solar radiation leading to higher temperature about 45℃. On the other hand, air around the water body has a lower temperature about 27-30℃. At the same time, the air layer near the external wall has higher temperature owing to the absorption and reflection of solar radiation on the wall. On the other hand, as the water body has lower temperature and been less affected by solar radiation, the cool air near the water surface lowers the air temperature above the water body though latent heat exchange. However, the affected area is mainly above the water body which indicates the cooling air cannot transfer to adjacent area as expected.

Figure 8 Temperature distribution in a longitudinal

section of samplingsampling area in Case B

Figure 9 shows water vapour mass fraction in a longitudinal section of samplingsampling area in Case B. It can be found that the maximum moisture is above water surface at the value of 0.022 kg/kg, 0.008 higher than inlet The building height and width near the water body have a greater impact on the moisture diffusion. Under the influence of the dominant wind, the water vapour flows over the low building near the water body (at the height of 20m) to the downwind area, and then blocked by high building, which indicates the higher the building is, the more difficult the water vapour transfer is.

Figure 9 Water vapour mass fraction in a

longitudinal section of samplingsampling area in

case B

As mentioned above, t_v and m_v are used to evaluate the thermal enviroment of differernt building distribution. Y represents distance from centre of water body and W represents the width of water body. All measuring points are 1.5m high from the ground.

Figure 10 shows the temperature distribution of four cases. It can be seen that regularity of cases remain same with lower temperature above water body and

higher temperature in building area. Case A and case C have relatively cooler airflow in building area of which building floor area ratio and height of buildings are both large. The temperature in Case D is highest above all as it has lower building floor area ratio and building height, which means that the ground and building surface gain more solar radiation to heat the air as there is less shade made by tall buildings.
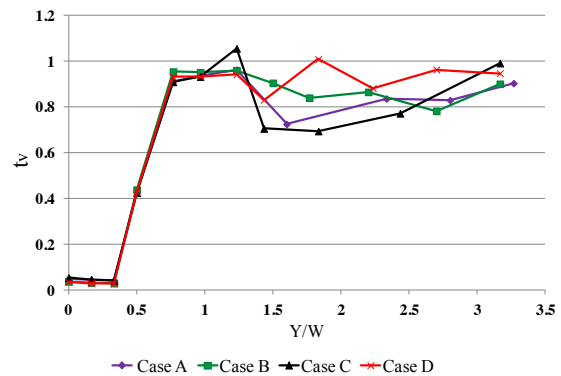

Figure 10 t_V vs. Y/W of the four cases

Figure 11 shows the humidity distribution of four cases. The distribution of each case is similar and all peak at the centre of water body. Then m_v drops dramatically with distance inceasing. Apart from temperature distribution, four cases show differernt potential on huimidity diffusion. It can be seen that reduction of humidity in Case D is minimum due to lower building height and building floor area ratio which allow water vapor diffusing more easily. On contrary, the worst performance appears in Case C, of which building shape is enclosed-type with large height leading to mass blocking for water vapor transfer.
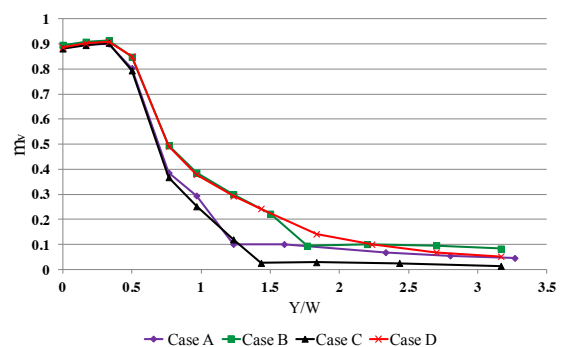

Figure 11 m_V vs. Y/W of the four cases

CONCLUSION

According to discussion mentioned above, all models match the experimental data well in predicting

thermal environment around water body. The result of LES matches the experimental data best followed by RSM. The S-A model shows the worst performance of prediction on thermal environment in whole area. The SKE model is adopted to evaluate thermal environment on full scale for time and energy saving. It is obvious that the layout of building arrays has significantly affected distribution of temperature and humidity separately. The prediction shows the cooling effect of water body has decreased less with higher building height, because of less shade made by tall buildings. Additionally, the spread length of humidity is obviously shortened by tall and enclosed-type building leading to mass blocking for water vapor diffusion. Therefore, a comprehensive index should be considered combining all factors of thermal environment including the effect of vegetation in order to obtain whole evaluation of cooling effect of water body in different building area in future work.

ACKNOWLEDGEMENT

REFERENCES

Akashi Mochida and Isaac Y.F.Lun. 2008. Prediction of wind environment and thermal comfort at pedestrian level in urban area. Journal of Wind Engineering and Industrial Aerodynamic.

Ashie, Y., and Kono, T. 2006. Environmental change due to the redevelopment in Shiodome area. Wind Engineers.

Badrinath N, Yau MK, and Schuepp PH. 2004. The effects of small water bodies on the atmospheric heat and water budgets over the MacKenzie Water body Basin. Hydrol Process.

Chen L. and Yu Z. 2007. Numerical modeling for the building performance of city underlying surface and thermal environments in WuHan, Master.thesis, Huazhong University of Science and Technology. China.

E.A. Hathway, S. Sharples. 2012. The interaction of river and urban form in mitigating the Urban Heat Island effect: A UK case study．Building and Environment.

Ken-ichi NARITA. 1992. Effects of river on urban thermal environment dependent on the types of on-shore building distribution, journal of architecture on planning environment. (In Japanese).

Richards P J, Hoxey R P.1993. Appropriate boundary conditions for computational wind engineering models using the k-ε model, Journal of Wind Engineering and Industrial Aerodynamics.

Zhao B. and Jiang Y. 2002. Optimized design of wind environment in building cluster by numerical simulation, Urban Planning Forum.